processes

MDPI

Article

Fe_3O_4@Granite: A Novel Magnetic Adsorbent for Dye Adsorption

Gamze Topal Canbaz

Department of Chemical Engineering, Faculty of Engineering, Sivas Cumhuriyet University, Sivas 58140, Turkey; gtopal@cumhuriyet.edu.tr

Abstract: Magnetic granite (MG), a new and low-cost adsorbent, was prepared by the chemical co-precipitation of Fe^{2+} and Fe^{3+} using granite (G), which is a magmatic rock type. The adsorption of the Reactive Black 5 (RB5) dye from aqueous solutions on Fe_3O_4-modified granite was examined in a batch system. Fourier transform infrared spectroscopy (FTIR), scanning electron microscopy (SEM), energy-dispersive X-ray (EDX), X-ray fluorescence spectrometry (XRF), X-ray diffractometry (XRD), N_2 adsorption–desorption, vibrating-sample magnetometry (VSM), and point-of-zero charge (pH_{pzc}) analysis were used to characterize the prepared MG. Magnetic granite displayed significant magnetization and could be easily separated using external magnets. The maximum adsorption capacity was 29.85 mg/g at 298 K. According to kinetic and isothermal examinations, the pseudo-second-order model and Langmuir isothermal adsorption were the best fit for adsorption. It was found that the enthalpy change ΔH (kJ/mol) was −31.76, and the entropy change ΔS (kJ/mol) was 0.096 for a temperature change of 298–330 K. The ΔG° (kJ/mol) value was negative at all temperatures (298 K, −2.86 kJ/mol; 303 K, −2.85 kJ/mol and 313 K, −1.50 kJ/mol), indicating that the adsorption of RB5 on MG was spontaneous.

Keywords: Reactive Black 5; magnetic granite; adsorption; Fe_3O_4; chemical co-precipitation

check for updates

Citation: Topal Canbaz, G. Fe_3O_4@Granite: A Novel Magnetic Adsorbent for Dye Adsorption. *Processes* **2023**, *11*, 2681. https://doi.org/10.3390/pr11092681

Academic Editor: Thomas S.Y. Choong

Received: 7 August 2023
Revised: 27 August 2023
Accepted: 4 September 2023
Published: 7 September 2023

1. Introduction

The dye content of wastewater from the paper, pharmaceutical, plastic, leather, and, especially, textile industries is very considerable. More than 1000 tons of dyes—45% of which are reactive dyes—are discharged into natural waters by the effluents of various enterprises each year [1]. Dyes take an important place in these sectors. Dyes belong to the class of aromatic and heterocyclic compounds with azo bonds (-N=N-) and exhibit toxic, mutagenic, and even carcinogenic properties. They cause considerable damage to the central nervous and digestive systems and the liver [2]. The discharge of untreated wastewater with high dye contents into the environment where living organisms are present is among the main sources of water pollution [3]. The above-mentioned negative properties impact the life system in nature, including plants, animals, and humans. Therefore, decolorizing wastewater from industries in which dyes are used is also important for the whole ecosystem [4].

Reactive Black 5 is a diazo acidic reactive dye known as Remazol Black B in the industry (Table 1). Reactive dyes are widely used due to their low cost, bright color, and the property of providing effective coloring by binding to materials through covalent bonds. Studies reported that prolonged exposure to RB5 may cause skin rashes, bladder cancer, chromosomal abnormalities, respiratory and kidney failure, and asthma [5–7]. Furthermore, reactive dyes are highly soluble in water. Therefore, it is challenging to remove them from wastewater using conventional methods [8].

Numerous methods have been reported in the literature for dye removal, such as electrocoagulation [9], the Fenton [10,11] and photocatalytic reaction [12–15], and adsorption [16,17]. Adsorption is preferred among the said methods because of its simple application, low cost, and reproducibility [16,18].

Table 1. The physical and chemical properties of the RB5 dye.

Chemical Name	Reactive Black 5 (Remazol Black B)
Chemical formula	$C_{26}H_{21}N_5Na_4O_{19}S_6$
Molecular weight	991.82 g/mol
Maximum absorbance	597 nm
Ionic structure	Anionic dye
Water solubility	Highly soluble
Molecular structure	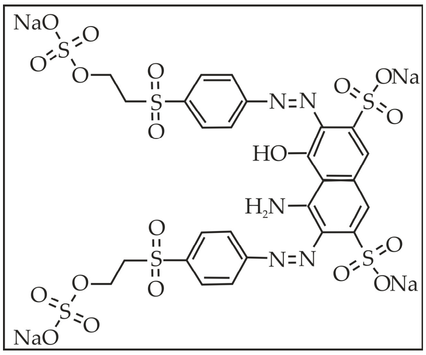

However, using the adsorption method, the efficient separation of adsorbents from water is difficult and may take a long time [19]. Fe_3O_4 magnetic particles are characterized by a large surface area and their easy separation from reaction media. The large surface area, biocompatibility, non-toxicity, and easy synthesis of Fe_3O_4 enable its use in various fields [20]. Magnetic particles and composite materials made with magnetic particles are considered potential materials for the removal of pollutants from aqueous media [21–25]. Magnetic materials are preferred to centrifugation or filtration separation methods as they are more effective, with respect to the time and the energy required, in adsorption processes [26]. After adsorption, magnetic materials containing the adsorbed compounds are separated by a magnet. This separation method is reported to be faster, safer, and more efficient than centrifugation and filtration [27–29].

Some studies were conducted on the removal of the RB5 dye from aqueous media using various adsorbents. Low-cost agricultural products [30–33], pumice [34], activated carbon [35], zeolite [8,36], clay [37], and various composite materials [38–40] were used for RB5 removal.

The present study used granite, a magmatic rock type, as the basic material constituting the adsorbent's structure [41]. Granite is a rock type comprising quartz and alkali feldspar from 20% to 60% [42]. To the best of our knowledge, no study in the literature has examined the use of granite or magnetic granite as an adsorbent. Granite was magnetized and used for RB5 removal. On the basis of its magnetic properties, it was separated from the environment quickly and without energy consumption after the process. The results showed that MG could be utilized as a novel alternative adsorbent in wastewater treatment.

2. Materials and Methods

2.1. Materials

The granite used in the study was obtained from the Davulalan region, Sivas. RB5 dye, $FeSO_4 \cdot 7H_2O$, $FeCl_3$, and NH_4OH were acquired from Sigma-Aldrich (St. Louis, MO, USA).

2.2. RB5 Stock Solution Preparation

The RB5 dye was utilized without any prior preparation. The stock solution used in the study was prepared at 1000 mg/L and diluted to the desired concentrations. The pH of the RB5 solutions was adjusted using 0.1 M NaOH and 0.1 M HCl.

2.3. Synthesis of Magnetic Granite (MG)

Magnetic granite was prepared by the co-precipitation method. $FeCl_3$ and $FeSO_4 \cdot 7H_2O$ were used, and the Fe^{2+}/Fe^{3+} mole ratio was adjusted to 1/2. The solution prepared with Fe^{2+} and Fe^{3+} (1:1 volume ratio) was stirred at 80 °C until homogenization. Then, 2.5 g of granite was added to the Fe^{2+} and Fe^{3+} solution, stirring at 80 °C for 2 h. In the end, 25% NH_4OH solution was slowly added to the mixture. The solution's color turned black, indicating that magnetic particles had formed. The residual ammonium ions were eliminated from the mixture by repeatedly washing it with distilled water. The washed magnetic granite particles were dried at 70 °C [43]. Figure 1 shows the synthesized MG.

Figure 1. MG under the external magnet effect.

2.4. Granite and Magnetic Granite Characterization

Granite and magnetic granite were characterized by FTIR, SEM, EDX, XRF, XRD, N_2 adsorption–desorption, VSM, and pHpzc.

The morphology of granite and magnetic granite was investigated using SEM and EDX for qualitative chemical analysis. For the purpose of identifying potential functional groups in the structures of granite and magnetic granite, FT-IR analysis in the 400–4000 cm^{-1} range was carried out. The elemental analyses of granite and magnetic granite were conducted by XRF. The crystal structure of granite and magnetic granite was determined by XRD. To determine the surface and pore characteristics, N_2 adsorption–desorption analysis was performed. The VSM analysis was conducted to identify the magnetic properties of magnetic granite.

2.5. RB5 Removal

A 100 ppm RB5 stock solution was prepared by dissolving 0.1 g of RB5 dye in 1 L of distilled water. Various parameters, such as pH (3.0–7.0), initial dye concentration (20–200 mg/L), adsorbent dosage (0.25–5 g/L), contact time (0–300 min), and temperature (25–40 °C), were examined. The "one-factor-at-a-time method" was employed to design the experimental system. The best parameter conditions were determined sequentially. Batch system experiments were conducted in a 50 mL volume. RB5 concentration was measured by determining the absorbance at 597 nm with a UV–visible spectrophotometer (Merck Spectroquant Pharo 300, KGaA, Darmstadt, Germany). The % removal efficiency and the adsorption capacity were determined according to the following equations (Equations (1) and (2)):

$$\text{Removal efficiency (\%)} = [(C_o - C_e)/C_o] \times 100 \quad (1)$$

$$q_e = \frac{(C_o - C_e)V}{m} \quad (2)$$

C_o refers to the initial concentration (mg/L), C_e is the concentration of the substance remaining unadsorbed at equilibrium (mg/L), V denotes the solution volume (L), and m represents the adsorbent dosage (g).

2.6. Reusability

We added 0.05 g of MG to 200 mg/L of RB5 solution and submitted it to the dye adsorption process for 120 min at ambient temperature (pH: 4.0). After this process, the desorption process with 0.1 M NaOH was applied to RB5-adsorbed MG to determine the desorption efficiency. After rinsing with distilled water to remove any remaining NaOH MG was dried in an oven. These processes were repeated five times, and the regeneration efficiency was calculated by Equation (3).

$$\text{Regeneration efficiency} = (\text{Amount of the dye desorbed}/\text{Amount of the dye adsorbed}) \times 100 \quad (3)$$

2.7. Mathematical Modeling of the Adsorption System

2.7.1. Adsorption Isotherms

The monolayer or multilayer adsorption of RB5 on MG was analyzed through the use of adsorption isotherms. The Langmuir, Freundlich, and Temkin isotherm models were used for the description of the adsorption system (Table 2).

Table 2. Adsorption isotherms and equations.

Isotherm Model	Equation	Reference
Langmuir Isotherm	$\frac{1}{q_e} = \frac{1}{q_m} + \frac{1}{b.q_m}\frac{1}{C_e}$	[44]
Freundlich Isotherm	$\ln q_e = \ln K_F + \frac{1}{n}\ln C_e$	[45]
Temkin Isotherm	$q_e = \frac{RT}{b_T}\ln(AC_e)$	[46]

2.7.2. Adsorption Kinetics

The adsorption kinetic model explained the adsorption mechanism, diffusion phenomena, and the connection between equilibrium time and adsorption capacity (Table 3).

Table 3. Kinetic models and equations.

Kinetic Model	Equation	Reference
Pseudo-first-order kinetic model	$\ln(qe - qt) = \ln qe - k_1 t$	[47]
Pseudo-second-order kinetic model	$\frac{t}{q_t} = \frac{1}{k_2 q_e{}^2} + \frac{1}{q_e}t$	[48,49]
Intraparticle diffusion	$q_t = k_d t^{1/2} + C$	[50]

2.7.3. Adsorption Thermodynamics

The Gibbs free energy change (ΔG°), enthalpy change (ΔH°), and entropy change (ΔS°) of RB5 adsorption were evaluated. The ΔG° value is essential since it indicates the spontaneity of a chemical reaction, which can be computed in the following way (Equation (4)):

$$\Delta G^\circ = -RT\ln K_c \quad (4)$$

where K_c ((amount of RB5 in the adsorbent)/(amount of RB5 in the solution)) represents the distribution coefficient.

The enthalpy change (ΔH) and entropy change (ΔS) were estimated from the equation below (Equation (5)):

$$\ln K_c = \frac{\Delta S}{R} - \frac{\Delta H}{RT} \quad (5)$$

3. Results

3.1. Characterization of Granite and Magnetic Granite

3.1.1. FTIR Results

A FTIR analysis was conducted with the objective of determining the functional groups in the material structure and explaining the interaction between the materials.

In the FTIR spectrum of granite (Figure 2), the bands at 3691 and 3615 cm^{-1} originate from the OH stretching of water in the layers of granite [51]. The peaks at 1797 cm^{-1} and 1442 cm^{-1} correspond to H-O-H bending vibrations and organic–inorganic hybrid bond peaks, respectively [52]. The stretching vibration of the Si-O-Si and Al-O-Si groups of aluminosilicate is related to the important peak at 1024 cm^{-1} in the IR spectra of granite [52,53]. This absorption band also indicates the presence of albite [26]. The medium band at 774 cm^{-1} is attributed to the Si-O-Si bond's tetrahedral bending vibration; this peak is representative of crystalline quartz [54]. The ring vibrations of framework silicates are responsible for the four extremely weak bands between 538 cm^{-1} and 700 cm^{-1} [53].

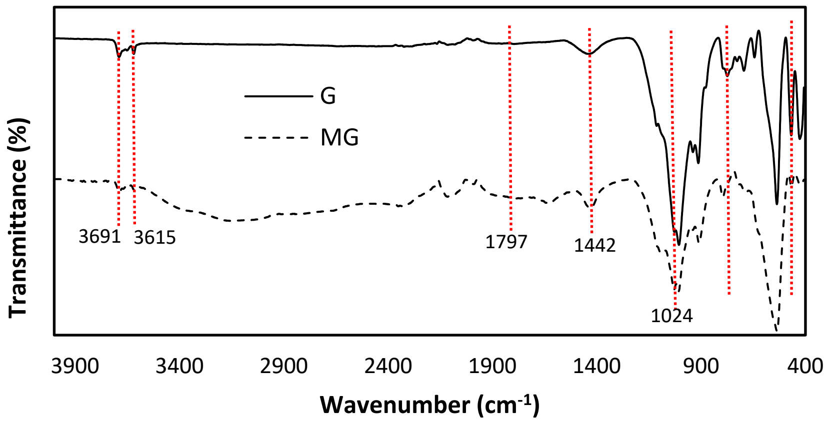

Figure 2. FTIR spectra of granite and magnetic granite.

Upon comparing the FTIR spectra of granite and magnetic granite, it was seen that the wave number did not change in many peaks. However, the transmittance values of the peaks in the magnetic granite spectrum were found to increase (Figure 2). These results showed that the internal structure of granite did not change following modification with iron [55–57].

The absorption peak of magnetic granite at ~550 cm^{-1} is the characteristic band of Fe-O stretching vibrations in Fe_3O_4 particles. It is possible to find the specific vibrations of Fe-O bonds around 460 cm^{-1} and 570 cm^{-1}. When the granite and magnetic granite peaks were compared, we observed that some peaks were shifted to new values while other peaks disappeared [56–58]. In fact, the peaks at 643 cm^{-1} and 783 cm^{-1} disappeared. These changes confirmed the modification with Fe_3O_4.

3.1.2. SEM-EDX Results

Figure 3 presents the SEM images of granite, magnetic granite, and magnetic granite after RB5 adsorption. The SEM image of granite shows that it had an agglomerated structure which did not display a homogeneous distribution. It was observed that spherical structures were formed when Fe_3O_4 was added to granite. A similar spherical structure was also observed in a kaolin-based magnetic zeolite [59]. After adsorption, the spherical structure decreased, and the gaps on the surface disappeared.

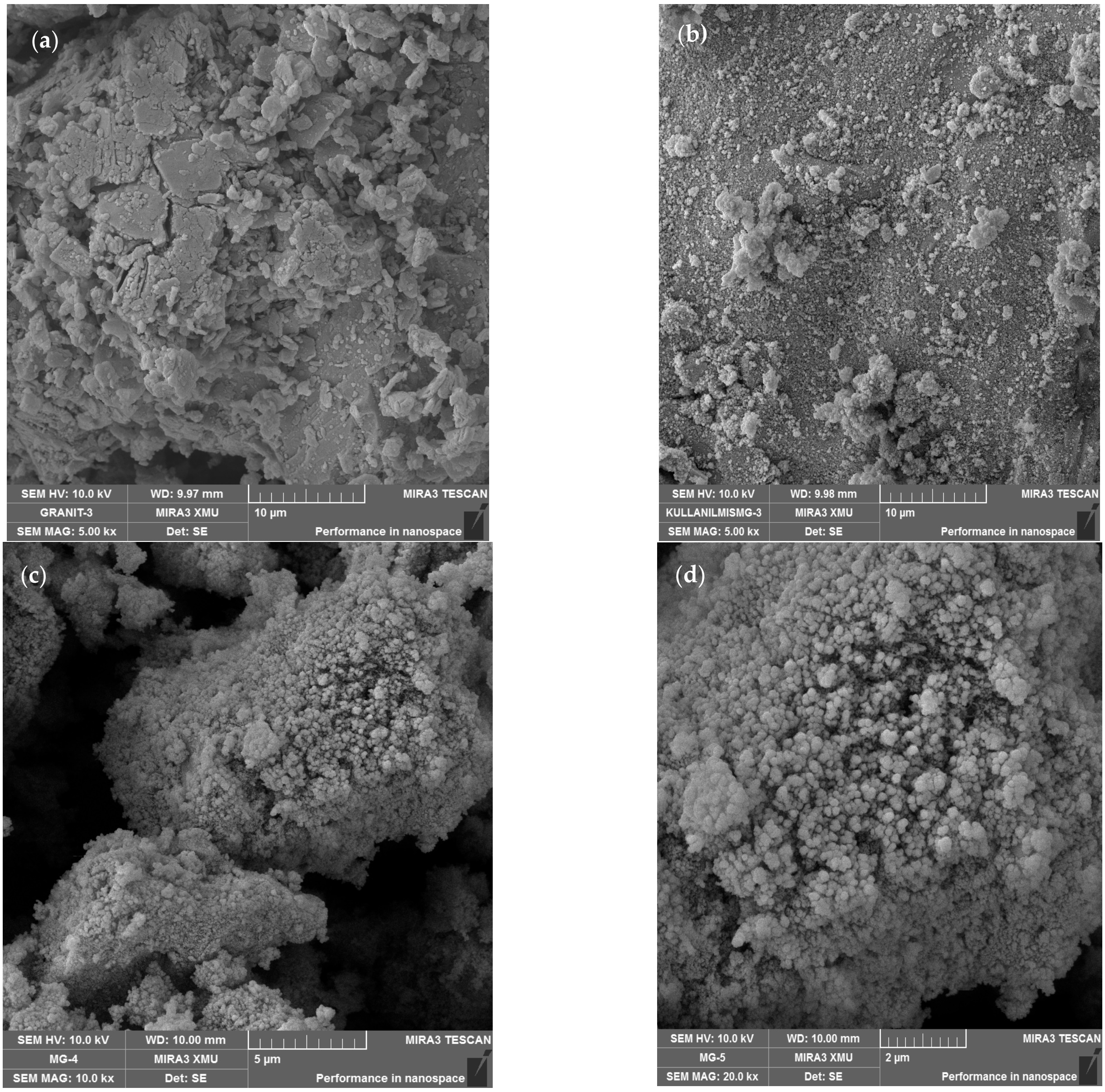

Figure 3. SEM images of granite (**a**), magnetic granite after RB5 adsorption (**b**), and magnetic granite (**c**,**d**).

Figure 4 shows the EDX analysis results of granite, MG, and RB5-adsorbed MG. In the EDX spectrum of granite, it was observed that the structure of granite mainly contained 55.43% O, 9.77% Al, and 23.72% Si as well as low amounts of Na, Mg, K, Ca, and Fe. The EDX spectrum analysis of MG, which was imparted magnetic properties by loading iron to granite, determined that 60.94% Fe was present. C, N, and S in the EDX spectrum of MG after adsorption derived from the RB5 dye, indicating that the RB5 dye was adsorbed by MG.

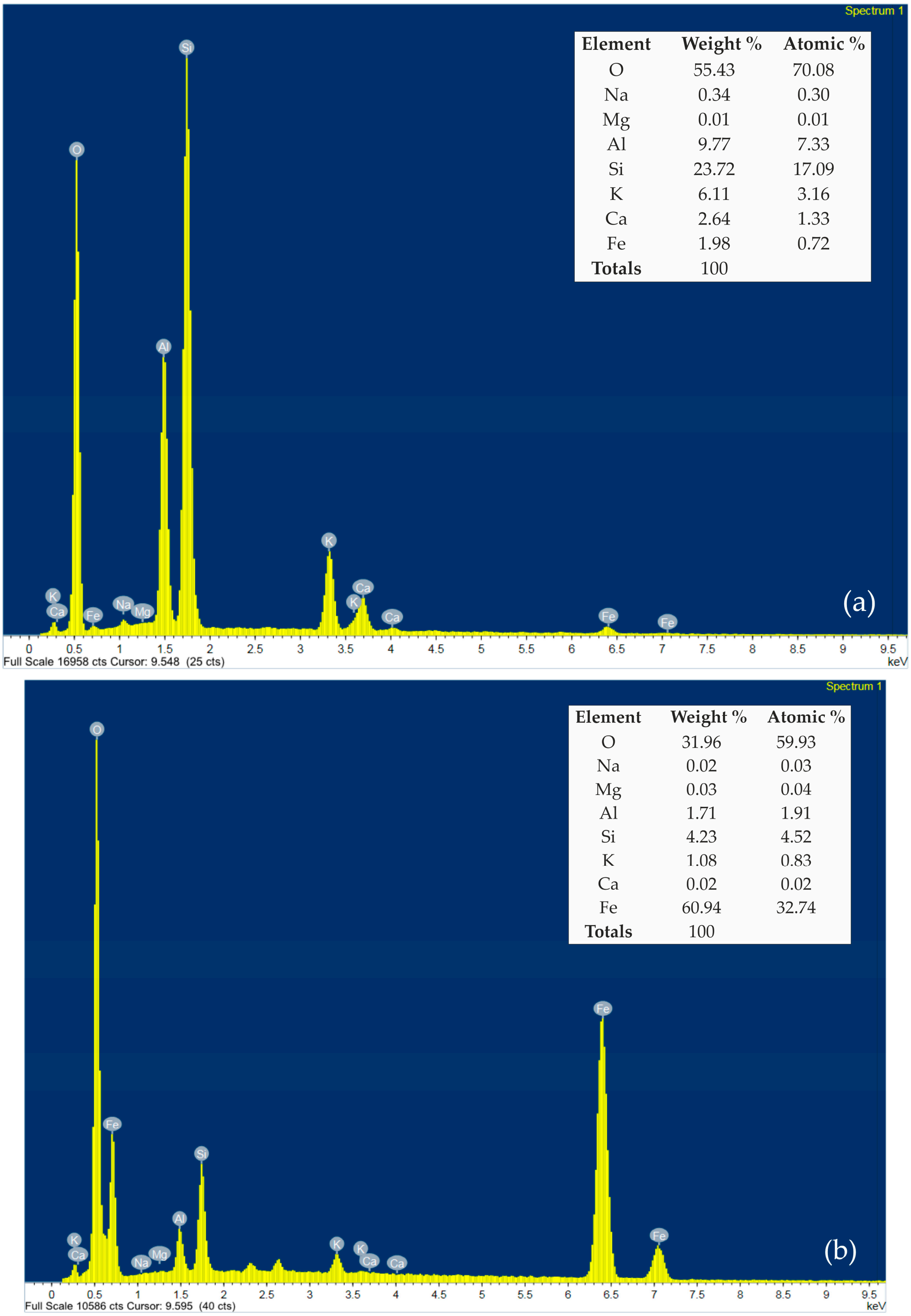

Figure 4. *Cont*.

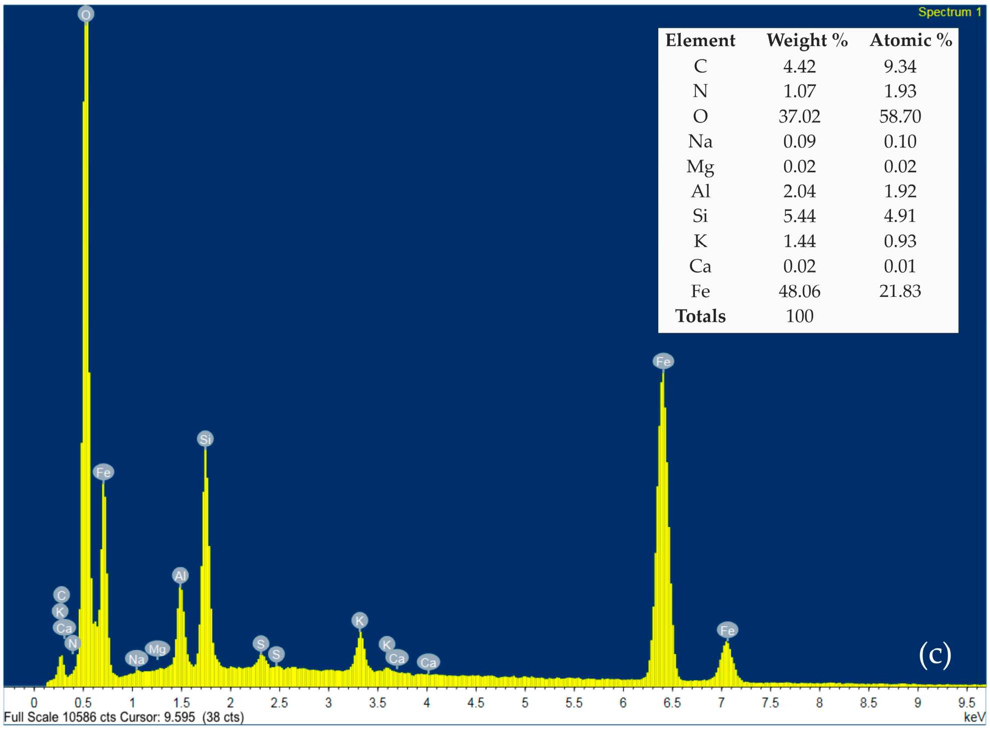

Figure 4. EDX results of granite (**a**), magnetic granite (**b**), and magnetic granite after RB5 adsorption (**c**).

3.1.3. XRF Results

An XRF analysis was carried out for the purpose of revealing the elemental composition of granite and magnetic granite (Table 4).

Table 4. XRF results of granite and magnetic granite.

	Element (%)												
	Mg	**Al**	**Si**	**Ti**	**V**	**Mn**	**Fe**	**Zn**	**Zr**	**Nb**	**Mo**	**Pb**	**Bi**
G	0.53	21.97	74.775	0.477	0.151	0.285	1.65	0.015	0.047	0.012	0.003	0.032	0.053
MG	0.15	5.14	16.97	0.111	0.03	0.16	77.41	0.01	0.02	0.005	0.002	0.032	0.02

The XRF analysis of granite showed that its elemental composition mainly consisted of Si (74.77%) and Al (21.97%). The granite structure contained a very low amount of Fe (1.65%). The percentage contents of the other elements in the table were determined as <1%.

In the XRF analysis of magnetic granite, the Fe (77.41%) ratio increased due to modification, whereas the Si (16.97%) and Al (5.14%) percentages decreased.

The elemental composition of granite and magnetic granite was determined by EDX and XRF analyses. In XRF analysis, analyzing elements with atomic numbers less than 11 is impossible. Therefore, the element "O" is not included in the XRF analysis results, which causes the percentages of elements in EDX and XRF analyses to differ.

Nevertheless, the EDX and XRF results showed a high proportion of Al and Si in the structure of granite and an increased proportion of Fe in the structure of magnetic granite, which was similar in the two analyses.

3.1.4. XRD Results

An XRD analysis was performed at 2θ = 0–65° to determine the crystal phase and structural features of granite and magnetic granite, and the results are presented in Figure 5.

The sharp peaks at 2θ = 20.9° and 26.54° are the characteristic peaks belonging to quartz in the granite structure [60]. The peak positions in the XRD pattern of granite were in line with the literature [60–63]. The peaks at 2θ = 30.26°, 35.6°, 43.32°, 57.36°, and 62.94° in the XRD pattern of iron-modified granite confirmed the addition of Fe_3O_4 to the granite structure [64].

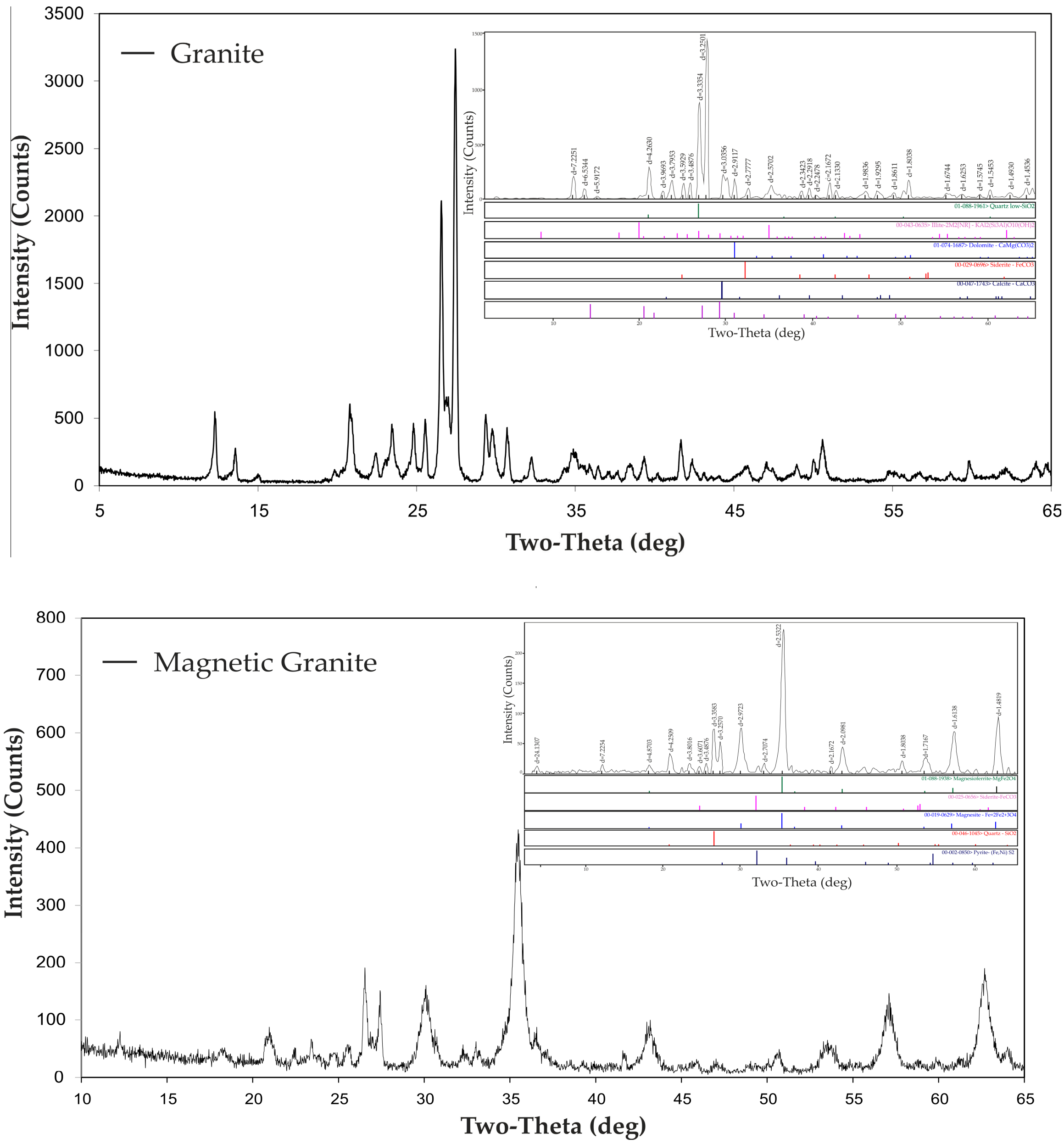

Figure 5. XRD patterns of granite and magnetic granite.

3.1.5. Adsorption–Desorption Analysis

Table 5 reports the surface area and pore sizes of granite and magnetic granite. According to the N_2 adsorption–desorption characterization results, the surface area of granite modified with Fe_3O_4 loading was determined by the BET and BJH methods. The surface area of magnetic granite was larger compared to that of granite. While the surface area of granite was 0.46 m^2/g, the surface area after iron loading was 19.12 m^2/g. The pore size measurement results showed that both materials were mesoporous (d = 2–50 nm).

Table 5. N_2 adsorption–desorption results of granite and magnetic granite.

		Granite	Magnetic Granite
Surface area (m^2/g)	Single-point surface area at P/Po	0.4532 m^2/g	19.0604 m^2/g
	BET Surface Area	0.4638 m^2/g	19.1211 m^2/g
	BJH adsorption cumulative surface area of pores with width between 17.000 Å and 3000.000 Å	0.1485 m^2/g	4.006 m^2/g
Pore volume (cm^3/g)	Single-point adsorption total pore volume of pores	0.000287 cm^3/g	0.013088 cm^3/g
	BJH Adsorption cumulative volume of pores with width between 17.000 Å and 3000.000 Å	0.000099 cm^3/g	0.004697 cm^3/g
Pore size (Å)	BJH Adsorption average pore width (4V/A)	39.137 Å	46.901 Å

The increase in the specific surface area with the addition of Fe_3O_4 could be attributed to the partial penetration of iron oxide into the granite layers, which led to the formation of new layers, increasing both the surface area and the interlayer porosity. These results agree with the studies reporting that the modification of a support with Fe_3O_4 increased surface area and pore size [56,65,66].

3.1.6. VSM Results

The magnetic characteristics of granite loaded with Fe_3O_4 were examined with a vibrating sample magnetometer operating between 0 and 15 K. The internal hysteresis loop of magnetic granite demonstrated an "S"-shaped curve at magnetic ambient temperature (Figure 6). The saturation magnetization (Ms) value of iron-modified granite was calculated as 46.04 emu/g, with a magnetization value of 3.5314 emu for 0.0767 g.

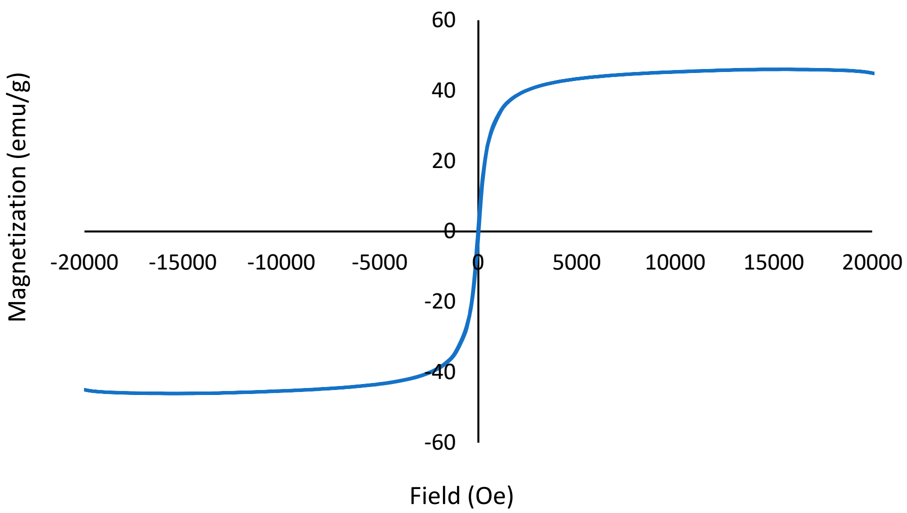

Figure 6. VSM curve of magnetic granite.

A study in the literature reported the Ms value of Fe_3O_4 nanoparticles and Fe_3O_4 in bulk form as 53.81 emu/g and 92 emu/g, respectively [67]. Another study found the MS value of Fe_3O_4 nanoparticles to be 59 emu/g. It was reported that when Fe_3O_4 nanoparticles were coated with chitosan, the MS value was 51.4 emu/g, and the polymer coating process reduced magnetization [68].

The VSM analysis determined the maximum field for iron-modified granite as 25,000 Oe, coercivity (Hci) as 24,515 Oe, and permanence (Mr) as 0.13901 emu. These values confirmed that iron-modified zeolite has adequate magnetic features to be attracted by a permanent magnet [69]. When the external magnetic field was removed, the particles were redispersed and reinstated [70].

3.2. Adsorption Studies

3.2.1. Effect of the Initial pH and of the pH_{PZC} of MG

A solution's pH is among the most significant parameters that impact adsorption, since it influences the degree of ionization, the surface charge of the adsorbent, and the structure of the dye to be removed. The effect of pH on the removal of RB5 dye from MG was studied in the pH range from 3 to 7, keeping constant the dye concentration (50 mg/L), the adsorbent dosage (1.5 g/L), the temperature (23 °C), and the contact time (240 min). The results obtained are presented in Figure 7. The adsorption capacity of the MG adsorbent was 25.99 mg/g and 25.53 mg/g at pH 3.0 and 4.0, respectively. The adsorption capacity decreased with an increasing pH of the solution. The lowest adsorption efficiency was 0.2 mg/g at pH 6.98, which was the pH value of the solution. Dye removal was favored at pH values of 3 and 4, and the subsequent experiments were performed at pH 4.0. Electrostatic attraction is stronger in acidic solutions due to the anionic SO_4^- centers in the structure of RB5, which leads to higher adsorption efficiency at low pH values [71].

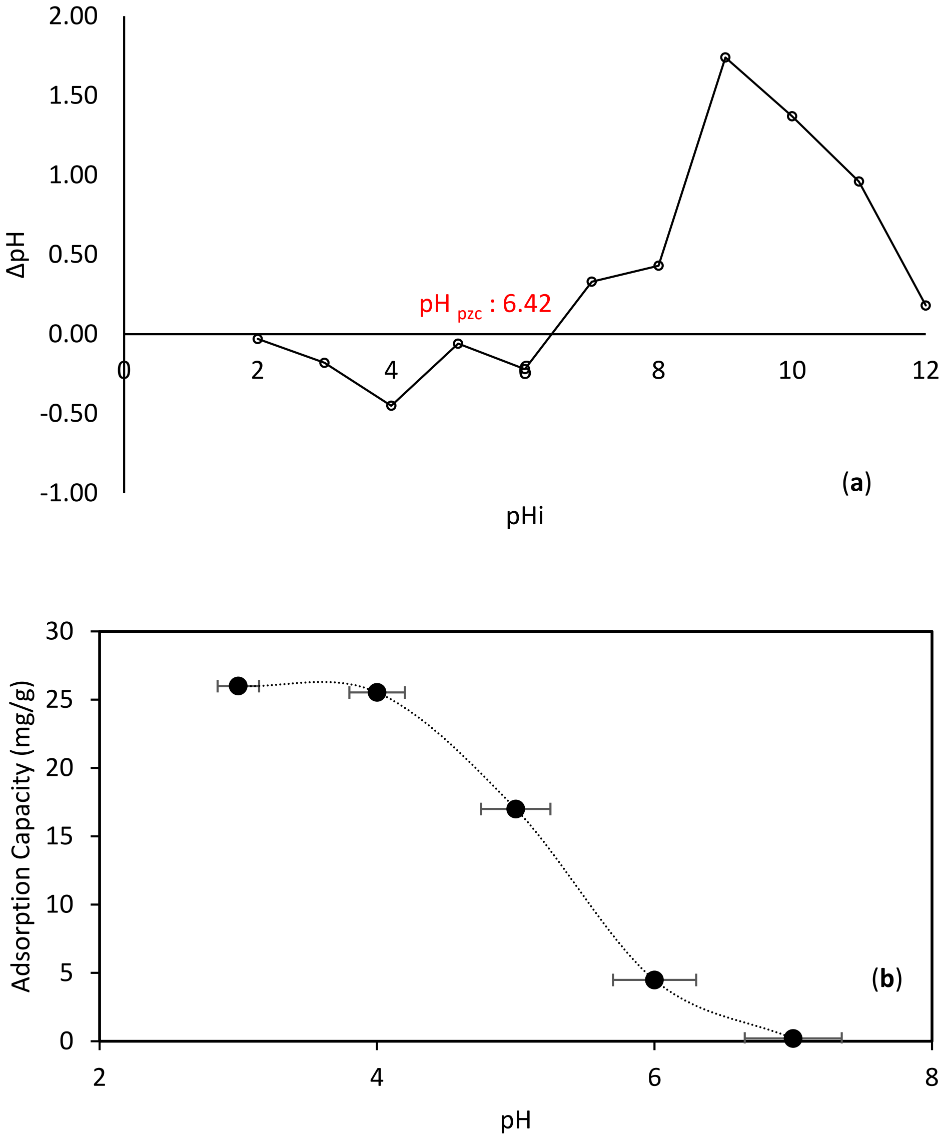

Figure 7. pH_{PZC} for MG (**a**) and the impact of pH on the adsorption of RB5 on MG (**b**) (RB5 concentration: 50 mg/L, adsorbent dosage: 1.5 g/L, T: 23 °C, t: 240 min).

The pH_{PZC} was determined to better define the adsorption mechanism. The surface charge of an adsorbent is positive at pH < pH_{PZC} and negative at pH > pH_{PZC} [72–76]. The

pH_{PZC} value of the MG adsorbent was found to be 6.42, and the MG surface charge was positive at pH < 6.42 and provided the maximum adsorption of RB5 dye, an anionic dye, at pH 4.0.

3.2.2. Effect of the Adsorbent Dosage

The effect of the adsorbent dosage on dye removal was studied in the range of 0.25–5 g/L, keeping constant the dye concentration (50 mg/L), the pH (4.0), the temperature (23 °C), and the contact time (240 min). Figure 8 shows the results of the removal of RB5 with MG. The removal percentage of RB5 dye increased with an increasing adsorbent dosage. The removal efficiency was determined to be 22.42% and 88.09% at 0.25 g/L and 5 g/L, respectively. Increasing the adsorbent dosage from 2.5 g/L to 5 g/L did not change the removal efficiency. The increased removal efficiency is also related to an increased number of active centers involved in the removal as the adsorbent dosage increases [77]. Figure 8 shows a decrease in the adsorption capacity of MG with the increase in the adsorbent amount. The adsorption capacity was found to be 45.93 mg/g and 9.02 mg/g at 0.25 g/L and 5 g/L, respectively. This explained why the unit adsorption capacity decreased with the increasing adsorbent dosage, since some areas on the adsorbent surface remained empty [78,79]. For the RB5 removal with MG, 2.5 g/L was determined as the adsorbent dosage, and further experiments were conducted with this amount.

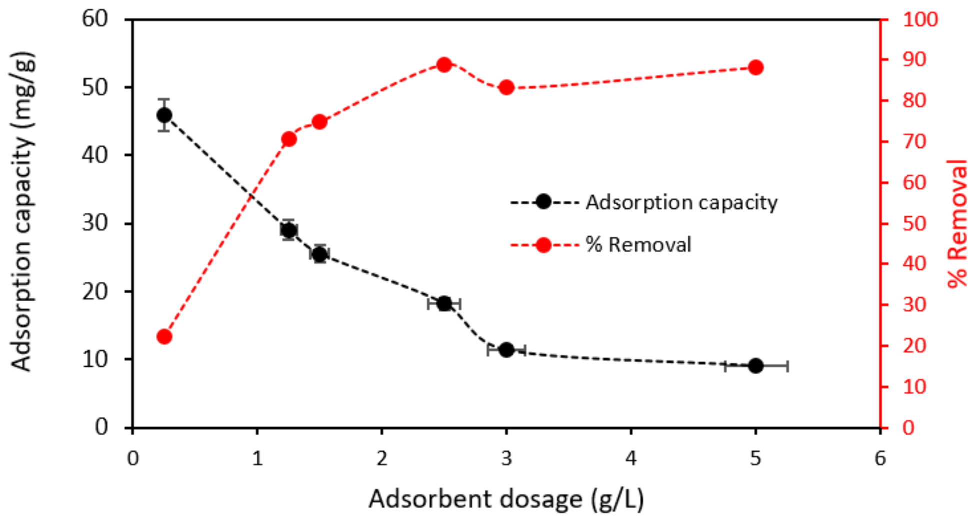

Figure 8. Effect of the adsorbent dosage on the adsorption of RB5 on MG (RB5 concentration: 50 mg/L, pH: 4.0, T: 23 °C, t: 240 min).

3.2.3. Effect of the Dye Concentration and Isotherm Modeling

The initial dye concentration in the removal of RB5 dye with MG was investigated at pH 4.0, with contact time of 240 min and 2.5 g/L of adsorbent. The RB5 concentration was studied in the 60–200 mg/L range. The calculated adsorption capacity was 17, 22, 23, 28, and 29 mg/g at initial dye concentrations of 60, 80, 100, 150, and 200 mg/L, respectively. The adsorption capacity increased with the increasing RB5 concentration, but no significant difference was observed in the presence of 150 and 200 mg/L contaminant concentrations (Figure 9). The saturation of the adsorption centers explains why the adsorption capacity does not change significantly at high concentrations [80]. The increasing dye concentration increased the required interaction forces by overcoming the resistance related to mass transfer between MG and RB5. Accordingly, a higher adsorption capacity was obtained [81].

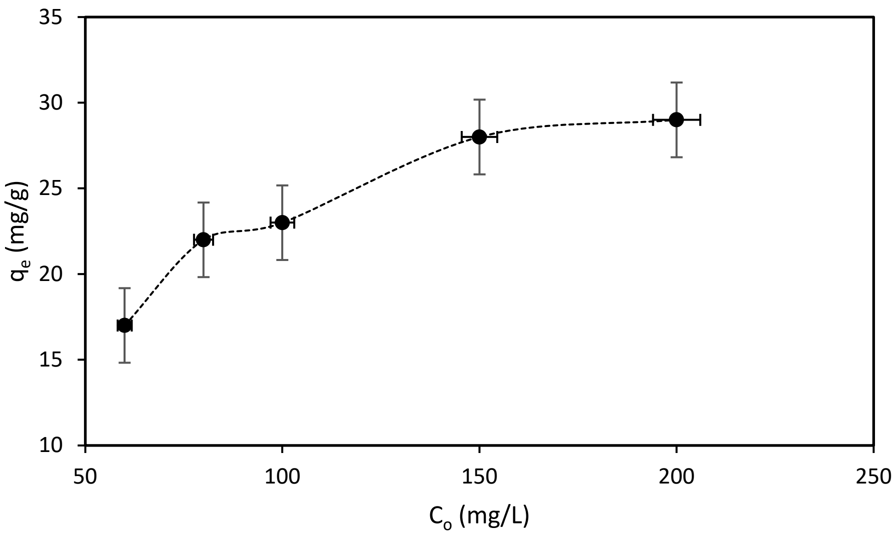

Figure 9. Effect of the initial RB5 concentration (pH: 4.0, adsorbent dosage: 2.5 g/L, T: 23 °C, t: 240 min).

The equilibrium data for RB5 removal with MG were characterized by the Langmuir, Freundlich, and Temkin isotherms (Figure 10). Table 6 reports Q_{max}, b, and the correlation coefficient computed from the Langmuir isotherm model, k_F and 1/n, and the A_t and b_t constants computed from the Temkin isotherm.

Table 6. The Langmuir, Freundlich, and Temkin isotherm constants for RB5 adsorption on MG.

	Isotherm Constants	298 K	303 K	313 K	323 K
Langmuir	Q_{max}	29.85	28.01	26.45	21.41
	b	0.121	0.113	0.057	0.143
	R^2	0.89	0.95	0.95	0.74
Freundlich	k_F	12.95	5.87	7.73	12.29
	1/n	0.16	0.39	0.22	0.10
	R^2	0.83	0.71	0.82	0.49
Temkin	A_t	12.46	0.29	1.84	653.76
	b_t	0.64	0.23	0.61	1.51
	R^2	0.86	0.60	0.84	0.47

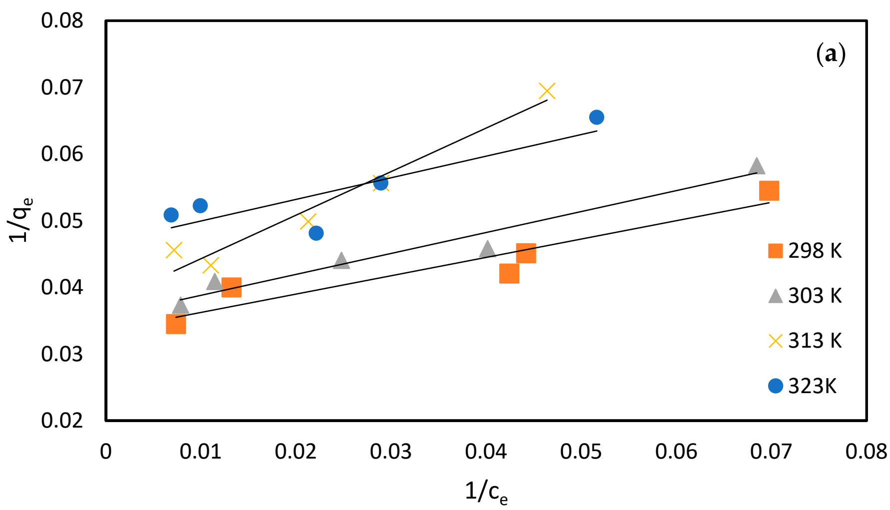

Figure 10. *Cont.*

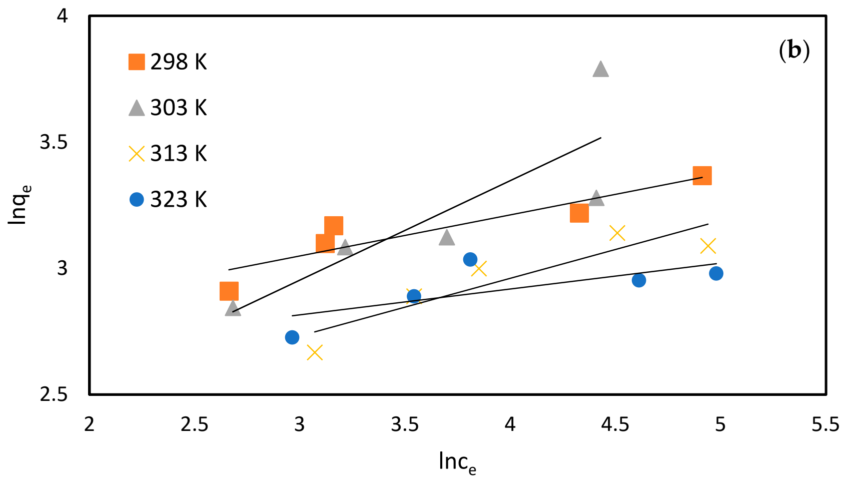

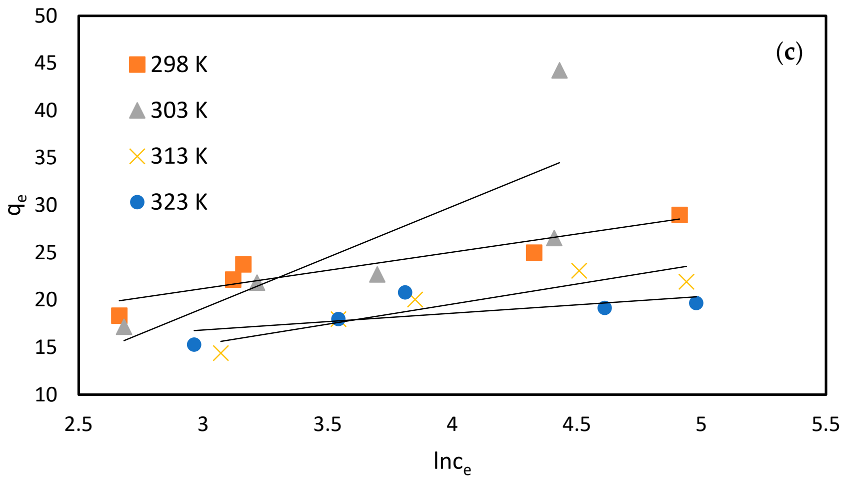

Figure 10. Adsorption isotherms: Langmuir (**a**), Freundlich (**b**), Temkin (**c**).

Table 7 reports the RB5 removal results with various adsorbents. The maximum adsorption capacity obtained at 298 K for RB5 removal with MG was 29.85 mg/g. As seen in the table, very different results were obtained because the parameters selected in each study were different. Table 7 allowed us to acquire an approximate idea of the results of RB5 removal with MG.

Table 7. RB5 removal with various adsorbents.

Adsorbent	q_e (mg/g)	Ref.
Magnetic iron oxide nanoparticles	18	[5]
ZnO–chitosan composite beads	189.44	[38]
Activated carbon (prepared from orange peel)	11.85	[82]
Brazilian pine-fruit shells (*Araucaria angustifolia*)	74.6	[32]
Activated carbon (prepared from Brazilian pine-fruit shells)	446.2	[32]
TiO_2-G5/PET films	155.04	[83]
Acidic modification of natural stone (pumice)	10	[84]
Polyacrylamide cryogels modified with polyethyleneimine	201	[85]
Cu/natural zeolite	0.4299	[86]
Surfactant-modified zeolite	12	[8]
Fly ash	7.93	[87]
Powdered activated carbon	58.52	[87]
Pre-treated *Aspergillus flavus*	26.95	[88]
Magnetic granite	29.85	This study

3.2.4. Contact Time's Effects and Kinetic Model

To study the impact of contact time on the adsorption of RB5 dye on MG, studies were performed at various contact times (5–300 min). Figure 11 displays the impact of the contact time on the adsorption capacity. The q_e-t graph shows an increase in the amount adsorbed as the contact time increased. The removal efficiencies for 30, 60, and 300 min were 60%, 70%, and 74%, respectively, for a 60 mg/L RB5 concentration, whereas the removal efficiencies for 30, 60, and 300 min were 28%, 28%, and 36%, respectively, for a 200 mg/L RB5 concentration. Very high removal rates were reached in the first minutes due to the high number of active sites. However, because of the decrease in and the occupancy of the said zones and the rapid equilibrium, the dye removal gradually decreased. The reason for this is the strong attraction force between dye molecules and adsorbent materials; intraparticle diffusion takes place after rapid surface diffusion. Similar results were obtained for RB5 removal using magnetic chitosan [89]. The equilibrium time for RB5 removal with MG was determined to be 60 min.

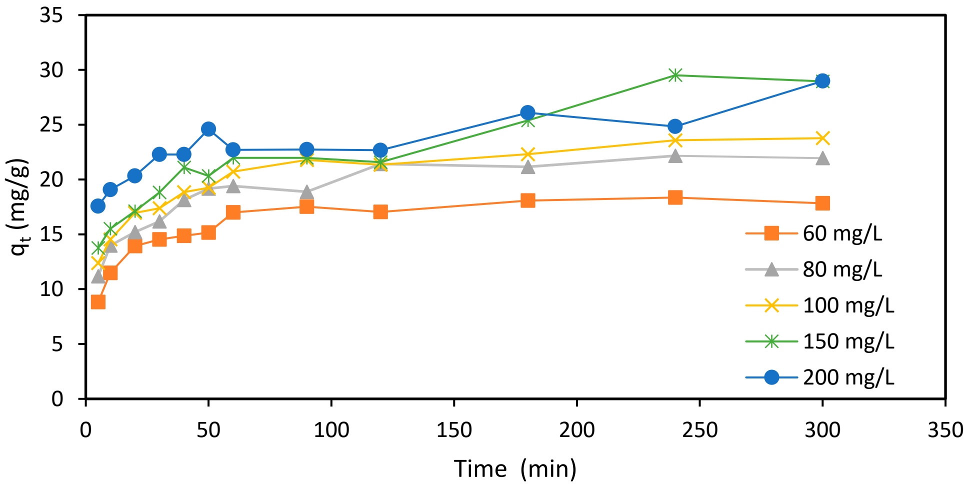

Figure 11. Effect of the contact time on RB5 adsorption.

Kinetic studies are essential for determining the best adsorption time of a pollutant on an adsorbent. The most commonly used kinetic models were analyzed to determine the kinetic parameters for RB5 dye adsorption on MG. Table 8 presents the data obtained from the PFO, PSO, and IPD kinetic models. Upon comparing the experimental q_e values obtained from the adsorption system with the calculated q_e values, the system was determined to be in accordance with the PSO kinetic model.

Table 8. Kinetic data for the adsorption of RB5 on MG.

T (K)	C_o (mg/L)	q_e (exp.) (mg/g)	Pseudo-First-Order			Pseudo-Second-Order			Inrtaparticle Diffusion		
			q_e (cal.) (mg/g)	k_1 (min^{-1})	R^2	q_e (cal.) (mg/g)	k_2 ($g \cdot mg^{-1} min^{-1}$)	R^2	k_i ($mg \cdot g^{-1} min^{-1/2}$)	C	R^2
298	60	18.35	4.60	0.0092	0.66	18.51	0.0044	0.99	1.416	−13.1	0.72
	80	22.16	7.10	0.0105	0.76	22.62	0.0046	0.99	0.644	12.69	0.81
	100	23.77	7.91	0.0103	0.77	24.27	0.0040	0.99	0.679	13.56	0.85
	150	25.39	8.27	0.0850	0.87	29.94	0.0017	0.98	0.969	13.00	0.93
	200	28.99	9.48	0.0059	0.78	25.44	0.0077	0.99	0.571	17.94	0.85

The intraparticle diffusion model was used to analyze the adsorption mechanism (Figure 12). The relationship between diffusion, equilibrium time, and adsorption capacity is described by investigating the adsorption mechanism. The adsorption of RB5 on MG was realized in two steps. In the first step, when adsorption took place, RB5 was adsorbed on the adsorbent surface. Most adsorption occurred in this first step, according to boundary layer diffusion. In the second step, the process was slower, as shown by the lower slope of the line. This step involved intraparticle diffusion. In the diffusion of RB5 on MG, boundary layer diffusion occurred in the first 60 min, and intraparticle diffusion occurred afterward. The equilibrium time of the adsorption system was determined to be 60 min.

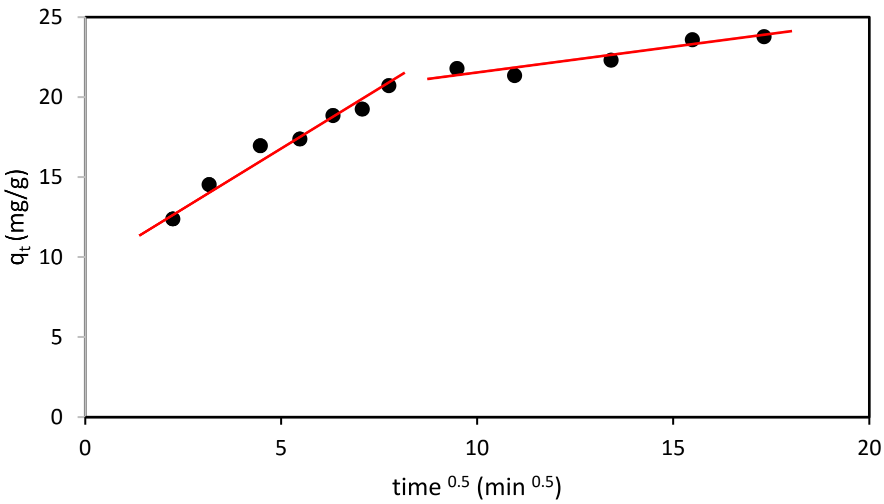

Figure 12. Intraparticle diffusion modeling of RB5 adsorbed on MG (pH: 4.0, adsorbent dosage: 2.5 g/L, T: 23 °C, C_o: 100 mg/L).

3.2.5. Temperature's Effects and Thermodynamic Parameters

The impact of temperature on the adsorption of RB5 on MG was studied in the range of 23–40 °C with 60–200 mg/L of RB5, at pH 4.0, and 0.25 g of adsorbent. The adsorption capacity was observed to decrease as the temperature increased (Figure 13). At the concentration of 200 mg/L RB5, the adsorption capacity was 28.99 mg/g at 23 °C, while the it decreased to 19.66 mg/g when the temperature increased to 50 °C. Likewise, at the concentration of 60 mg/L RB5, the adsorption capacity was 18.35 mg/g at 23 °C and decreased to 12.26 mg/g as the temperature increased to 50 °C. The decreased adsorption capacity with the increasing temperature indicated that the system was exothermic.

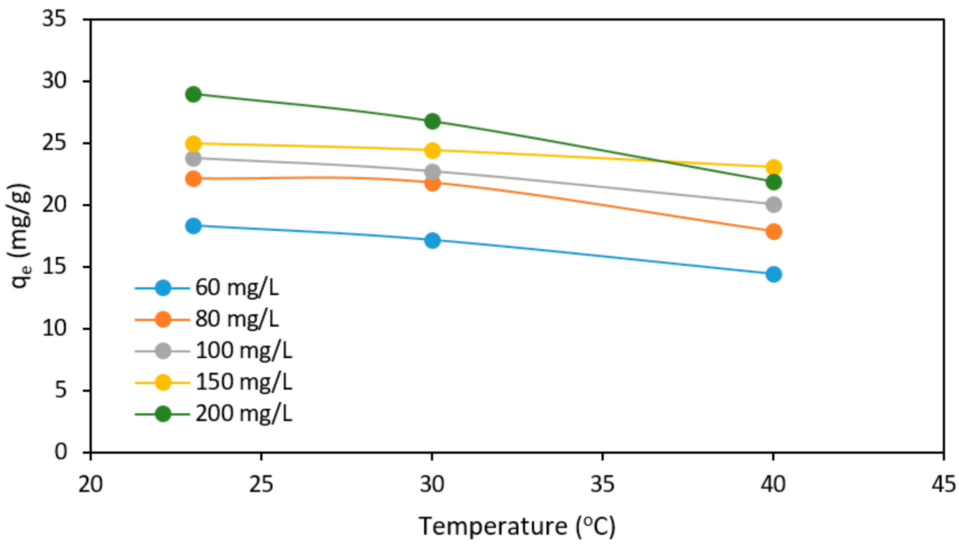

Figure 13. Effect of temperature on RB5 adsorption.

Thermodynamic parameters, such as ΔG, ΔH, and ΔS, were calculated for RB5 adsorption with magnetic granite. The experiments were conducted at 25–40 °C with 60 mg/L of

RB5. Table 9 shows the calculated ΔG, ΔH, and ΔS values. The negative ΔH values at all temperatures and concentrations showed that the adsorption was exothermic. The negative ΔG values demonstrated that the adsorption was spontaneous.

Table 9. Thermodynamic parameters for RB5 adsorption with magnetic granite.

Temperature (K)	ΔG° (kJ/mol)	ΔH° (kJ/mol)	ΔS° (kJ/mol K)	R^2
298	−2.86			
303	−2.85	−31.76	0.096	0.90
313	−1.50			

3.3. Regeneration

The adsorbent's regeneration is an important factor in the efficiency and economy of an adsorptive process. The regeneration of the used adsorbent and the reuse of the regenerated adsorbent in adsorption systems are important from an environmental and economic point of view. To determine the reusability of MG used in the study, 0.1 M NaOH was used as an eluent for the regeneration process.

MG used for RB5 adsorption was oven-dried at 50 °C for 3 h in the regeneration experiments. In the first cycle after regeneration, it was determined that magnetic granite removed 85.06% of RB5 (Figure 14). In the 5th cycle, the RB5 removal rate decreased to 49.15%. The results obtained proved that MG is reusable.

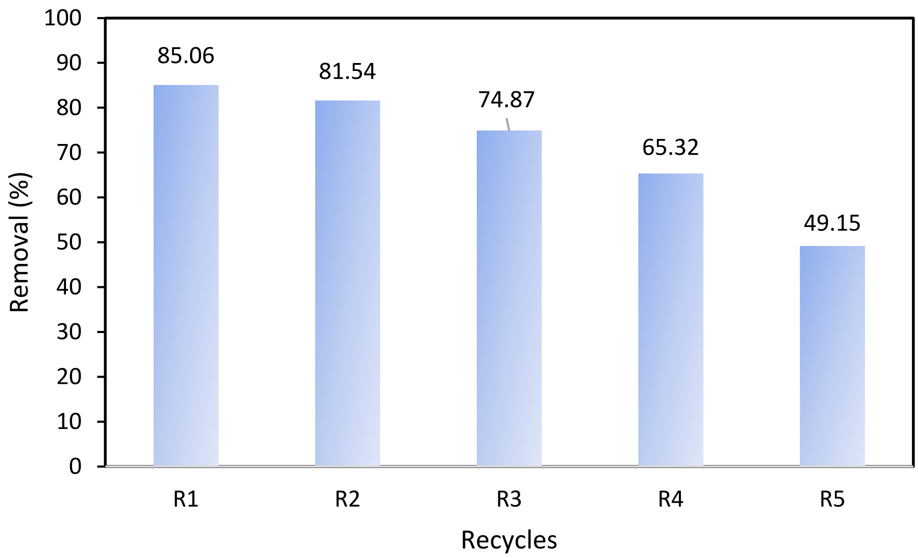

Figure 14. Reusability of MG.

4. Conclusions

In this study, magnetic granite was synthesized using natural rock-type granite by the chemical co-precipitation method for RB5 adsorption. The characterization results showed the success of magnetization. Magnetic granite was found to have a larger surface area (G: 0.4638 m^2/g, MG: 19.1211 m^2/g) than granite. According to the VSM results for MG, the saturation magnetization (Ms) value was 46.04 emu/g. The presence of Fe_3O_4 peaks in the XRD pattern of magnetic granite proved that Fe_3O_4 was added to the granite structure. The spectra obtained from FTIR analysis also confirmed the modification with Fe_3O_4. In the EDX analysis of MG, the peaks appearing after adsorption confirmed RB5 adsorption. The adsorption of RB5 on magnetic granite showed a good fit with the Langmuir isotherm model and the pseudo-second-order kinetic model. The adsorption of magnetic granite was spontaneous and exothermic. This research demonstrated that magnetic granite could be efficiently utilized for RB5 adsorption from textile wastewater.

Funding: This research received no external funding.

Data Availability Statement: The data presented in this study are available on request from the corresponding author.

Conflicts of Interest: The author declares no conflict of interest.

References

1. Sarvestani, M.R.J.; Doroudi, Z. Removal of Reactive Black 5 from Waste Waters by Adsorption: A Comprehensive Review. *J. Water Environ. Nanotechnol.* **2020**, *5*, 180–190.
2. El-Zawahry, M.M.; Abdelghaffar, F.; Abdelghaffar, R.A.; Hassabo, A.G. Equilibrium and Kinetic Models on the Adsorption of Reactive Black 5 from Aqueous Solution Using Eichhornia Crassipes/chitosan Composite. *Carbohydr. Polym.* **2016**, *136*, 507–515. [CrossRef] [PubMed]
3. Munagapati, V.S.; Wen, J.C.; Pan, C.L.; Gutha, Y.; Wen, J.H.; Reddy, G.M. Adsorptive Removal of Anionic Dye (Reactive Black 5) from Aqueous Solution Using Chemically Modified Banana Peel Powder: Kinetic, Isotherm, Thermodynamic, and Reusability Studies. *Int. J. Phytoremediation* **2020**, *22*, 267–278. [CrossRef] [PubMed]
4. Correia, V.M.; Stephenson, T.; Judd, S.J. Characterisation of Textile Wastewaters—A Review. *Environ. Technol.* **1994**, *15*, 917–929. [CrossRef]
5. Chang, M.; Shih, Y. Synthesis and Application of Magnetic Iron Oxide Nanoparticles on the Removal of Reactive Black 5: Reaction Mechanism, Temperature and pH Effects. *J. Environ. Manag.* **2018**, *224*, 235–242. [CrossRef]
6. Chompuchan, C.; Satapanajaru, T.; Suntornchot, P.; Pengthamkeerati, P. Decolorization of Reactive Black 5 and Reactive Red 198 Using Nanoscale Zerovalent Iron. *World Acad. Sci. Eng. Technol.* **2009**, *37*, 130–134.
7. Jafari, A.J.; Kakavandi, B.; Kalantary, R.R.; Gharibi, H.; Asadi, A.; Azari, A.; Babaei, A.A.; Takdastan, A. Application of Mesoporous Magnetic Carbon Composite for Reactive Dyes Removal: Process Optimization Using Response Surface Methodology. *Korean J. Chem. Eng.* **2016**, *33*, 2878–2890. [CrossRef]
8. Karadag, D.; Turan, M.; Akgul, E.; Tok, S.; Faki, A. Adsorption Equilibrium and Kinetics of Reactive Black 5 and Reactive Red 239 in Aqueous Solution onto Surfactant-Modified Zeolite. *J. Chem. Eng. Data* **2007**, *52*, 1615–1620. [CrossRef]
9. Mook, W.T.; Aroua, M.K.; Szlachta, M.; Lee, C.S. Optimisation of Reactive Black 5 Dye Removal by Electrocoagulation Process Using Response Surface Methodology. *Water Sci. Technol.* **2017**, *75*, 952–962. [CrossRef]
10. Meriç, S.; Kaptan, D.; Ölmez, T. Color and COD Removal from Wastewater Containing Reactive Black 5 Using Fenton's Oxidation Process. *Chemosphere* **2004**, *54*, 435–441. [CrossRef]
11. Domenzain-Gonzalez, J.; Castro-Arellano, J.J.; Galicia-Luna, L.A.; Rodriguez-Cruz, M.; Hernandez-Lopez, R.T.; Lartundo-Rojas, L. Photocatalytic Membrane Reactor Based on Mexican Natural Zeolite: RB5 Dye Removal by Photo-Fenton Process. *J. Environ. Chem. Eng.* **2021**, *9*, 105281. [CrossRef]
12. Mathiarasu, R.R.; Manikandan, A.; Panneerselvam, K.; George, M.; Raja, K.K.; Almessiere, M.A.; Slimani, Y.; Baykal, A.; Asiri, A.M.; Kamal, T.; et al. Photocatalytic Degradation of Reactive Anionic Dyes RB5, RR198 and RY145 via Rare Earth Element (REE) Lanthanum Substituted $CaTiO_3$ Perovskite Catalysts. *J. Mater. Res. Technol.* **2021**, *15*, 5936–5947. [CrossRef]
13. Nassehinia, H.; Rahmani, H.; Rahmani, K.; Rahmani, A. Solar Photocatalytic Degradation of Reactive Black 5: By-Products, Bio-Toxicity, and Kinetic Study. *Desalin. Water Treat.* **2020**, *206*, 385–395. [CrossRef]
14. Inam, H.; Fatima, U.; Shahid, S.; Mansoor, S.; Yasin, A.; Javed, M.; Iqbal, S.; Alhujaily, A.; Althobiti, R.A.; Alzahrani, E.; et al. Nanotheranostic Fabrication of Iron Oxide for Rapid Photocatalytic Degradation of Organic Dyes and Antifungal Potential. *J. Saudi Chem. Soc.* **2023**, *27*, 101689. [CrossRef]
15. Aroosh, K.; Javed, M.; Hussain, N.; Alhujaily, A.; Iqbal, S.; Alotaibi, M.T.; Faizan, M.; Khan, M.S.; Bahadur, A.; Qayyum, M.A.; et al. Construction of Te-ZnO@S-G-C3N4Heterojunction Nanocomposites for the Efficient Removal of Methylene Blue, Antifungal Activity, and Adsorption of Cr(VI) Ion. *Adsorpt. Sci. Technol.* **2023**, *2023*, 6736182. [CrossRef]
16. Wong, S.; Ghafar, N.A.; Ngadi, N.; Razmi, F.A.; Inuwa, I.M.; Mat, R.; Amin, N.A.S. Effective Removal of Anionic Textile Dyes Using Adsorbent Synthesized from Coffee Waste. *Sci. Rep.* **2020**, *10*, 2928. [CrossRef] [PubMed]
17. Amin, M.T.; Alazba, A.A.; Shafiq, M. Adsorptive Removal of Reactive Black 5 from Wastewater Using Bentonite Clay: Isotherms, Kinetics and Thermodynamics. *Sustainabiliy* **2015**, *7*, 15302–15318. [CrossRef]
18. Raza, S.; Yong, X.; Yang, B.; Xu, R.; Deng, J. Biomass Trans-Anethole-Based Hollow Polymer Particles: Preparation and Application as Sustainable Absorbent. *ACS Sustain. Chem. Eng.* **2017**, *5*, 10011–10018. [CrossRef]
19. Sanad, M.M.S.; Farahat, M.M.; Abdel Khalek, M.A. One-Step Processing of Low-Cost and Superb Natural Magnetic Adsorbent: Kinetics and Thermodynamics Investigation for Dye Removal from Textile Wastewater. *Adv. Powder Technol.* **2021**, *32*, 1573–1583. [CrossRef]
20. Abutaleb, A.; Imran, M.; Zouli, N.; Khan, A.H.; Hussain, S.; Ali, M.A.; Bakather, O.; Gondal, M.A.; Khan, N.A.; Panchal, H.; et al. Fe_3O_4-Multiwalled Carbon Nanotubes-Bentonite as Adsorbent for Removal of Methylene Blue from Aqueous Solutions. *Chemosphere* **2023**, *316*, 137824. [CrossRef] [PubMed]
21. Li, C.; Dong, Y.; Yang, J.; Li, Y.; Huang, C. Modified Nano-graphite/Fe_3O_4 Composite as Efficient Adsorbent for the Removal of Methyl Violet from Aqueous Solution. *J. Mol. Liq.* **2014**, *196*, 348–356. [CrossRef]

22. Mohammed, A.A.; Samaka, I.S. Bentonite Coated with Magnetite Fe_3O_4 Nanoparticles as a Novel Adsorbent for Copper (II) Ions Removal from Water/wastewater. *Environ. Technol. Innov.* **2018**, *10*, 162–174. [CrossRef]
23. Tanhaei, B.; Ayati, A.; Bamoharram, F.F.; Lahtinen, M.; Sillanpää, M. A Novel Magnetic Preyssler Acid Grafted Chitosan Nano Adsorbent: Synthesis, Characterization and Adsorption Activity. *J. Chem. Technol. Biotechnol.* **2016**, *91*, 1452–1460. [CrossRef]
24. Mallakpour, S.; Hatami, M. An Effective, Low-Cost and Recyclable Bio-Adsorbent Having Amino Acid Intercalated LDH@Fe_3O_4/PVA Magnetic Nanocomposites for Removal of Methyl Orange from Aqueous Solution. *Appl. Clay Sci.* **2019**, *174*, 127–137. [CrossRef]
25. Chang, J.; Ma, J.; Ma, Q.; Zhang, D.; Qiao, N.; Hu, M.; Ma, H. Adsorption of Methylene Blue onto Fe_3O_4/activated Montmorillonite Nanocomposite. *Appl. Clay Sci.* **2016**, *119*, 132–140. [CrossRef]
26. Raza, S.; Yong, X.; Raza, M.; Deng, J. Synthesis of Biomass Trans-Anethole Based Magnetic Hollow Polymer Particles and Their Applications as Renewable Adsorbent. *Chem. Eng. J.* **2018**, *352*, 20–28. [CrossRef]
27. Wu, W.; He, Q.; Jiang, C. Magnetic Iron Oxide Nanoparticles: Synthesis and Surface Functionalization Strategies. *Nanoscale Res. Lett.* **2008**, *3*, 397–415. [CrossRef] [PubMed]
28. Zhu, H.; Zhang, M.; Liu, Y.; Zhang, L.; Han, R. Study of Congo Red Adsorption onto Chitosan Coated Magnetic Iron Oxide in Batch Mode. *Desalin. Water Treat.* **2012**, *37*, 46–54. [CrossRef]
29. Fang, Y.; Wu, X.; Dai, M.; Lopez-Valdivieso, A.; Raza, S.; Ali, I.; Peng, C.; Li, J.; Naz, I. The Sequestration of Aqueous Cr(VI) by Zero Valent Iron-Based Materials: From Synthesis to Practical Application. *J. Clean. Prod.* **2021**, *312*, 127678.
30. Wong, S.; Tumari, H.H.; Ngadi, N.; Mohamed, N.B.; Hassan, O.; Mat, R.; Saidina Amin, N.A. Adsorption of Anionic Dyes on Spent Tea Leaves Modified with Polyethyleneimine (PEI-STL). *J. Clean. Prod.* **2019**, *206*, 394–406. [CrossRef]
31. Çelebi, H. The Applicability of Evaluable Wastes for the Adsorption of Reactive Black 5. *Int. J. Environ. Sci. Technol.* **2019**, *16*, 135–146. [CrossRef]
32. Cardoso, N.F.; Pinto, R.B.; Lima, E.C.; Calvete, T.; Amavisca, C.V.; Royer, B.; Cunha, M.L.; Fernandes, T.H.M.; Pinto, I.S. Removal of Remazol Black B Textile Dye from Aqueous Solution by Adsorption. *Desalination* **2011**, *269*, 92–103. [CrossRef]
33. Kapoor, R.T.; Rafatullah, M.; Siddiqui, M.R.; Khan, M.A.; Sillanpää, M. Removal of Reactive Black 5 Dye by Banana Peel Biochar and Evaluation of Its Phytotoxicity on Tomato. *Sustainability* **2022**, *14*, 4176. [CrossRef]
34. Heibati, B.; Rodriguez-Couto, S.; Amrane, A.; Rafatullah, M.; Hawari, A.; Al-Ghouti, M.A. Uptake of Reactive Black 5 by Pumice and Walnut Activated Carbon: Chemistry and Adsorption Mechanisms. *J. Ind. Eng. Chem.* **2014**, *20*, 2939–2947. [CrossRef]
35. Vojnović, B.; Cetina, M.; Franjković, P.; Sutlović, A. Influence of Initial pH Value on the Adsorption of Reactive Black 5 Dye on Powdered Activated Carbon: Kinetics, Mechanisms, and Thermodynamics. *Molecules* **2022**, *27*, 1349. [CrossRef] [PubMed]
36. Kim, S.A.; Kamala-Kannan, S.; Oh, S.G.; Cho, M.; Bae, S.; Oh, B.T. Simultaneous Removal of chromium(VI) and Reactive Black 5 Using Zeolite Supported Nano-Scale Zero-Valent Iron Composite. *Environ. Earth Sci.* **2016**, *75*, 447. [CrossRef]
37. Ouakouak, A.; Abdelhamid, M.; Thouraya, B.; Chahinez, H.O.; Hocine, G.; Hamdi, N.; Syafiuddin, A.; Boopathy, R. Development of a Novel Adsorbent Prepared from Dredging Sediment for Effective Removal of Dye in Aqueous Solutions. *Appl. Sci.* **2021**, *11*, 10722. [CrossRef]
38. Çınar, S.; Kaynar, Ü.H.; Aydemir, T.; Çam Kaynar, S.; Ayvacıklı, M. An Efficient Removal of RB5 from Aqueous Solution by Adsorption onto Nano-ZnO/Chitosan Composite Beads. *Int. J. Biol. Macromol.* **2017**, *96*, 459–465. [CrossRef]
39. Coura, J.C.; Profeti, D.; Profeti, L.P.R. Eco-Friendly Chitosan/quartzite Composite as Adsorbent for Dye Removal. *Mater. Chem. Phys.* **2020**, *256*, 123711. [CrossRef]
40. Bhaumik, M.; Maity, A.; Gupta, V.K. Synthesis and Characterization of Fe0/TiO_2 Nano-Composites for Ultrasound Assisted Enhanced Catalytic Degradation of Reactive Black 5 in Aqueous Solutions. *J. Colloid Interface Sci.* **2017**, *506*, 403–414. [CrossRef]
41. Khalil, M.; Hanif, M.A.; Rashid, U.; Ahmad, J.; Alsalme, A.; Tsubota, T. Low-Cost Novel Nano-Constructed Granite Composites for Removal of Hazardous Terasil Dye from Wastewater. *Environ. Sci. Pollut. Res.* **2022**, *30*, 81333–81351. [CrossRef] [PubMed]
42. Haldar, S.K.; Tišljar, J. *Introduction to Mineralogy and Petrology*; Elsevier: Amsterdam, The Netherlands, 2013; ISBN 9780124081338.
43. Majid, Z.; AbdulRazak, A.A.; Noori, W.A.H. Modification of Zeolite by Magnetic Nanoparticles for Organic Dye Removal. *Arab. J. Sci. Eng.* **2019**, *44*, 5457–5474. [CrossRef]
44. Langmuir, I. The Adsorption of Gases on Plane Surfaces of Glass, Mica and Platinum. *J. Am. Chem. Soc.* **1918**, *40*, 1361–1403. [CrossRef]
45. Freundlich, H.M.F. Over the Adsorption in Solution. *J. Phys. Chem.* **1906**, *57*, 1100–1107.
46. Said, K.A.M.; Ismail, N.Z.; Jama'in, R.L.; Alipah, N.A.M.; Sutan, N.M.; Gadung, G.G.; Baini, R.; Zauzi, N.S.A. Application of Freundlich and Temkin Isotherm to Study the Removal of Pb(II) via Adsorption on Activated Carbon Equipped Polysulfone Membrane. *Int. J. Eng. Technol.* **2018**, *7*, 91–93. [CrossRef]
47. Lagergren, S. Zur Theorie Der Sogenannten Adsorption Geloster Stoffe. *Handlingar* **1898**, *24*, 1–39.
48. Ho, Y.S.; McKay, G. Pseudo-Second Order Model for Sorption Processes. *Process Biochem.* **1999**, *34*, 451–465. [CrossRef]
49. Ho, Y.S.; McKay, G. The Kinetics of Sorption of Divalent Metal Ions onto Sphagnum Moss Peat. *Water Res.* **2000**, *34*, 735–742. [CrossRef]
50. Choy, K.K.H.; Porter, J.F.; Mckay, G. Intraparticle Diffusion in Single and Multicomponent Acid Dye Adsorption from Wastewater onto Carbon. *Chem. Eng. J.* **2004**, *103*, 133–145. [CrossRef]
51. Hass Caetano Lacerda, E.; Monteiro, F.C.; Kloss, J.R.; Fujiwara, S.T. Bentonite Clay Modified with Nb2O5: An Efficient and Reused Photocatalyst for the Degradation of Reactive Textile Dye. *J. Photochem. Photobiol. A Chem.* **2020**, *388*, 112084. [CrossRef]

52. Aroke, U.O.; Abdulkarim, A.; Ogubunka, R.O. Fourier-Transform Infrared Characterization of kaolin, Granite, Bentonite and Barite. *J. Chem. Inf. Model.* **2013**, *53*, 1689–1699.
53. Tchadjié, L.N.; Djobo, J.N.Y.; Ranjbar, N.; Tchakouté, H.K.; Kenne, B.B.D.; Elimbi, A.; Njopwouo, D. Potential of Using Granite Waste as Raw Material for Geopolymer Synthesis. *Ceram. Int.* **2016**, *42*, 3046–3055. [CrossRef]
54. Schiavon, N. Kaolinisation of Granite in an Urban Environment. *Environ. Geol.* **2007**, *52*, 333–341. [CrossRef]
55. Samarghandi, M.R.; Al-Musawi, T.J.; Mohseni-Bandpi, A.; Zarrabi, M. Adsorption of Cephalexin from Aqueous Solution Using Natural Zeolite and Zeolite Coated with Manganese Oxide Nanoparticles. *J. Mol. Liq.* **2015**, *211*, 431–441. [CrossRef]
56. Mersin, G.; Açıkel, Ü.; Levent, M. Efficient Adsorption of Basic Blue 41 from Textile Wastewaters by Natural and Magnetically Modified Manisa-Gördes Clinoptilolite. *Chem. Eng. Process. Process Intensif.* **2021**, *169*, 108632. [CrossRef]
57. Cao, J.; Sun, Q.; Wang, P.; Shen, J.; Dai, X. Synthesize and Characterize of Fe_3O_4/zeolite 4A Magnetic Nanocomposite. *J. Dispers. Sci. Technol.* **2022**, *43*, 517–525. [CrossRef]
58. Ahangaran, F.; Hassanzadeh, A.; Nouri, S. Surface Modification of Fe_3O_4@SiO_2 Microsphere by Silane Coupling Agent. *Int. Nano Lett.* **2013**, *3*, 1–5. [CrossRef]
59. De Andrade Bessa, R.; de Sousa Costa, L.; Oliveira, C.P.; Bohn, F.; do Nascimento, R.F.; Sasaki, J.M.; Loiola, A.R. Kaolin-Based Magnetic Zeolites A and P as Water Softeners. *Microporous Mesoporous Mater.* **2017**, *245*, 64–72. [CrossRef]
60. Wu, H.; Zhao, X.; Wang, W.; He, B.; Geng, R.; Fan, Q. Interaction Mechanism of Radioactive Cesium on Beishan Granite. *Sci. Sin. Chim.* **2019**, *49*, 165–174. [CrossRef]
61. Bakruddin, B.; Sembiring, A.R. Minerals Identification and Analysis of Granite Rocks in South Aceh District Using X-ray Diffraction (XRD). *J. Inotera* **2019**, *4*, 79. [CrossRef]
62. Pernyeszi, T.; Farkas, R.; Kovács, J. Methylene Blue Adsorption Study on Microcline Particles in the Function of Particle Size Range and Temperature. *Minerals* **2019**, *9*, 555. [CrossRef]
63. Guo, Z.; Li, J.; Song, Y.; He, C.; Zhang, F. The Size Effect and Microstructure Changes of Granite after Heat Treatment. *Adv. Mater. Sci. Eng.* **2021**, *2021*, 9958255. [CrossRef]
64. Afshin, S.; Rashtbari, Y.; Vosoughi, M.; Rehman, R.; Ramavandi, B.; Behzad, A.; Mitu, L. Removal of Basic Blue-41 Dye from Water by Stabilized Magnetic Iron Nanoparticles on Clinoptilolite Zeolite. *Rev. Chim.* **2020**, *71*, 218–229. [CrossRef]
65. Louhichi, S.; Ghorbel, A.; Chekir, H.; Trabelsi, N.; Khemakhem, S. Properties of Modified Crude Clay by Iron and Copper Nanoparticles as Potential Hydrogen Sulfide Adsorption. *Appl. Clay Sci.* **2016**, *127–128*, 123–128. [CrossRef]
66. Shikuku, V.O.; Mishra, T. Adsorption Isotherm Modeling for Methylene Blue Removal onto Magnetic Kaolinite Clay: A Comparison of Two-Parameter Isotherms. *Appl. Water Sci.* **2021**, *11*, 103. [CrossRef]
67. Mohammadi, A.; Barikani, M. Synthesis and Characterization of Superparamagnetic Fe_3O_4 Nanoparticles Coated with Thiodiglycol. *Mater. Charact.* **2014**, *90*, 88–93. [CrossRef]
68. Zhu, A.; Yuan, L.; Liao, T. Suspension of Fe_3O_4 Nanoparticles Stabilized by Chitosan and O-Carboxymethylchitosan. *Int. J. Pharm.* **2008**, *350*, 361–368. [CrossRef] [PubMed]
69. Eskandari, L.; Kheiri, F.; Iravani, M.; Sirousazar, M. Synthesis, Characteristics and Kinetic Study of Magnetic-Zeolite Nano Composite for Adsorption of Zirconium. *Pet. Coal* **2018**, *60*, 1120–1131.
70. Chen, Y.; Liu, K. Magnetic Ce-Doped TiO_2/$NiFe_2O_4$/diatomite Ternary Composite: Enhanced Visible-Light-Driven Photocatalytic Performance. *Powder Technol.* **2017**, *313*, 44–53. [CrossRef]
71. Silva, T.C.; Fraga, T.J.M.; Carvalho, M.; Silva, V.L.; Da Motta, M.A. Removal of the Reactive Remazol Black B And Remazol Red from Aqueous Solutions by Adsorption onto Treated Residue from the Aluminum Industry. *Lat. Am. Appl. Res.* **2018**, *48*, 101–106. [CrossRef]
72. Zimmer, G.; Brauch, H.-J.; Sontheimer, H. Activated-Carbon Adsorption of Organic Pollutants. In *Sorbents Materials for Controlling Environmental Pollution, Current State and Trends*; Elsevier: Amsterdam, The Netherlands, 1988; pp. 579–596.
73. Newcombe, G.; Hayes, R.; Drikas, M. Granular Activated Carbon: Importance of Surface Properties in the Adsorption of Naturally Occurring Organics. *Colloids Surf. A Physicochem. Eng. Asp.* **1993**, *78*, 65–71. [CrossRef]
74. Benammar, S.; Haffas, M.; Hamitouche, A.; Boudjemaa, A.; Bachari, K. Relevance of Anethum Graveolens to Remove Rhodamine B in Aqueous Solution: Characterization, Kinetic and Isotherm Study. *React. Kinet. Mech. Catal.* **2023**, *136*, 465–490. [CrossRef]
75. Keskin, Z.S.; Mine Şenol, Z.; Kaya, S.; Şimşek, S. Prunus Mahaleb Shell as a Sustainable Bioresource for Carminic Acid Removal from Aqueous Solution: Experimental and Theoretical Studies. *J. Mol. Struct.* **2023**, *1275*, 134618. [CrossRef]
76. El Messaoudi, N.; El Khomri, M.; Chegini, Z.G.; Bouich, A.; Dbik, A.; Bentahar, S.; Labjar, N.; Iqbal, M.; Jada, A.; Lacherai, A. Dye Removal from Aqueous Solution Using Nanocomposite Synthesized from Oxalic Acid-Modified Agricultural Solid Waste and $ZnFe_2O_4$ Nanoparticles. *Nanotechnol. Environ. Eng.* **2022**, *7*, 797–811. [CrossRef]
77. Javanbakht, V.; Ghoreishi, S.M.; Habibi, N.; Javanbakht, M. A Novel Magnetic Chitosan/clinoptilolite/magnetite Nanocomposite for Highly Efficient Removal of Pb(II) Ions from Aqueous Solution. *Powder Technol.* **2016**, *302*, 372–383. [CrossRef]
78. Sharifi, M.J.; Nouralishahi, A.; Hallajisani, A.; Askari, M. Magnetic Chitosan Nanocomposites as Adsorbents in Industrial Wastewater Treatment: A Brief Review. *Cellul. Chem. Technol.* **2021**, *55*, 185–205. [CrossRef]
79. Reddy, P.M.K.; Verma, P.; Subrahmanyam, C. Bio-Waste Derived Adsorbent Material for Methylene Blue Adsorption. *J. Taiwan Inst. Chem. Eng.* **2016**, *58*, 500–508. [CrossRef]
80. Ozmen, M.; Can, K.; Arslan, G.; Tor, A.; Cengeloglu, Y.; Ersoz, M. Adsorption of Cu(II) from Aqueous Solution by Using Modified Fe_3O_4 Magnetic Nanoparticles. *Desalination* **2010**, *254*, 162–169. [CrossRef]

81. Şentürk, İ.; Alzein, M. Adsorptive Removal of Basic Blue 41 Using Pistachio Shell Adsorbent—Performance in Batch and Column System. *Sustain. Chem. Pharm.* **2020**, *16*, 100254. [CrossRef]
82. Bayrak, Y.; Uzgör, R. Removal of Remazol Black B Textile Dye from Aqueous Solution by Adsorption: Equilibrium and Thermodynamic Studies. *J. Dispers. Sci. Technol.* **2013**, *34*, 828–833. [CrossRef]
83. Santos, R.; Silva, É.F.M.; Dantas, E.J.M.; Oliveira, E.D.C.; Simões, T.B.; Araújo, Í.R.S.; Ribeiro, A.T.S.; Oliveira, L.P.S.; Garcia, R.R.P.; Almeida, L.C. Potential Reuse of PET Waste Bottles as a Green Substrate/Adsorbent for Reactive Black 5 Dye Removal. *Water. Air. Soil Pollut.* **2020**, *231*, 533. [CrossRef]
84. Soleimani, H.; Sharafi, K.; Amiri Parian, J.; Jaafari, J.; Ebrahimzadeh, G. Acidic Modification of Natural Stone for Remazol Black B Dye Adsorption from Aqueous Solution—Central Composite Design (CCD) and Response Surface Methodology (RSM). *Heliyon* **2023**, *9*, e14743. [CrossRef]
85. Gün Gök, Z.; İnal, M. Effective Removing of Remazol Black B by the Polyacrylamide Cryogels Modified with Polyethyleneimine. *J. Polym. Environ.* **2022**, *30*, 151–163. [CrossRef]
86. Lestari, D.Y.; Laksono, E.W.; Ikhsan, J.; Rohaeti, E. Modified Natural Zeolite as Adsorbent for Remazol Black B Dye: Kinetics and Equilibrium Aspects. *AIP Conf. Proc.* **2023**, *2556*, 040011.
87. Eren, Z.; Acar, F.N. Adsorption of Reactive Black 5 from an Aqueous Solution: Equilibrium and Kinetic Studies. *Desalination* **2006**, *194*, 1–10. [CrossRef]
88. Alaguprathana, M.; Poonkothai, M.; Ameen, F.; Ahmad Bhat, S.; Mythili, R.; Sudhakar, C. Sodium Hydroxide Pre-Treated Aspergillus Flavus Biomass for the Removal of Reactive Black 5 and Its Toxicity Evaluation. *Environ. Res.* **2022**, *214*, 113859. [CrossRef] [PubMed]
89. Elwakeel, K.Z. Removal of Reactive Black 5 from Aqueous Solutions Using Magnetic Chitosan Resins. *J. Hazard. Mater.* **2009**, *167*, 383–392. [CrossRef] [PubMed]